Letter

Complex-frequency calculation in acoustics with real-frequency solvers

Shuowei An [1], Tuo Liu [2,3,*], Jie Zhu [4,†] and Li Cheng [1,‡]

[1] *Department of Mechanical Engineering, Hong Kong Polytechnic University, Hong Kong, China*

[2] *Key Laboratory of Noise and Vibration Research, Institute of Acoustics, Chinese Academy of Sciences, Beijing 100190, China*

[3] *State Key Laboratory of Acoustics, Institute of Acoustics, Chinese Academy of Sciences, Beijing 100190, China*

[4] *Institute of Acoustics, School of Physics Science and Engineering, Tongji University, Shanghai 200092, China*

(Received 8 July 2024; revised 3 December 2024; accepted 3 January 2025; published 16 January 2025)

Complex-frequency calculation enables the characterization of open wave systems in the complex frequency plane as well as the evaluation of wave behaviors under virtual gain and/or loss, which has widespread applications in the investigations of wave scattering and non-Hermitian physics. The corresponding calculation approaches, however, have not been well developed and are usually limited to simple analytical models. Here, we report an efficient numerical method for calculating complex-frequency acoustic wave fields, in which the imaginary part of the frequency is equivalently converted into the variation in material parameters. In this way, the complex-frequency problem becomes a real-frequency one which can then be readily implemented with most existing numerical solvers of the Helmholtz equation. The proposed method is validated by considering two representative examples: the scattering of a one-port lossy acoustic resonator and the imaging of a lossy acoustic superlens under complex frequency excitation. Our work provides a practical and general solution for complex-frequency calculation, in principle, applicable to any complex, dispersive wave systems, which could serve as a powerful tool for fundamental and applied research related to wave scattering and non-Hermiticity.

DOI: 10.1103/PhysRevB.111.L020301

Introduction. The eigenvalues of a system's scattering matrix, together with their evolution within the complex frequency plane, provide rich information about the scattering behaviors, in which scattering singularities, known as poles and zeros corresponding to entirely divergent (purely outgoing) and vanished (purely incoming) wave states, can fully describe the resonant and scattering properties of the system. Complex frequency plane analysis of the scattering matrix has thus been commonly considered as an efficient approach to the exploration of various anomalous phenomena and effects associated with wave scattering or open systems, including but not limited to bound states in the continuum (BICs), exceptional points (EPs), superscattering, coherent perfect absorption (CPA), and CPA-Lasing, etc. [1–8]. For example, the merging and disappearance of a zero and a pole in an open Hermitian system suggests the emergence of a BIC upon continuous parameter tuning [1]; the coalescence of zeros (or poles) under non-Hermitian modulation signifies a scattering (or resonant) EP [9–11]. The design and optimization of wave-absorbing materials or structures are another typical scenario in which the complex frequency plane analysis of scattering zeros shows ever-growing importance in recent years [4,6,12,13]. However, explicit expression of a scattering matrix is usually necessary to create its complex frequency plane due to the lack of numerical solvers supporting complex-frequency calculation. This remains challenging for the study of more sophisticated or realistic systems with irregular geometries, complex dispersion and boundary conditions, and gain-loss modulation.

Another emerging direction involving complex frequency calculation and analysis is the intriguing system response or wave propagation behavior at complex frequencies with the imaginary frequency playing the role of virtual loss or gain [14–18] to the system. The idea has attracted great attention across a wide variety of fields and has been the key ingredient to demonstrate virtual parity-time (PT) symmetry [19], critical coupling and CPA [20–24] as well as the overcoming of intrinsic losses in the non-Hermitian skin effect [17], superlensing [14,15,25], sensing [18], and plasmonic [16] systems. The practical realization of complex-frequency excitation usually relies on either truncated temporally decaying/growing sinusoidal signal [14,17] or the synthesized multifrequency steady-state wave of its Fourier transform [15,16]. So do the corresponding numerical calculations and analyses, though simplified analytical models may be derived as an alternative approach. Those approximate treatments regarding complex frequency wave suffer from inevitable information loss, high computational costs, insufficient modeling, and cumbersome postprocessing, especially when dealing with practical structures.

Apart from the above two major topics, complex-frequency calculation can, in principle, serve as a powerful toolbox for the investigation of wave physics related to non-Hermiticity that induces complex-valued, nonorthogonal eigenstates [2,26] and various *PT*-symmetric [27,28] or topological phase transitions [2,29–31]. In this letter, we propose a numerical method compatible with most real-frequency solvers

*Contact author. liutuo@mail.ioa.ac.cn

†Contact author. jiezhu@tongji.edu.cn

‡Contact author. li.cheng@polyu.edu.hk

of Helmholtz equation for complex-frequency calculation in acoustics through transforming the imaginary-frequency component into equivalent material properties. We examine the applicability and validity of the proposed method in two classes of problems: the complex frequency plane analysis of a one-port resonant scattering system and the complex frequency wave propagation in a lossy holey-structured metamaterial. We consider well-established models that have been thoroughly investigated in many previous works, in which good agreement can be found between the results from our method and those from analytical solutions or the data in existing literature. Our proposed method is general and flexible, appliable to the analysis of any non-Hermitian acoustic systems, even with complex gain-loss modulations, boundary conditions and dispersion. It could also be extended to other wave systems or other forms of equations after further derivation.

Theory. We start with the inhomogeneous Helmholtz equation that describes linear acoustic waves in fluids in the frequency domain [32] with harmonic time dependence $e^{i\omega^* t}$:

$$\nabla \cdot \left(-\frac{1}{-\rho^*} (\nabla p - \boldsymbol{q}_d) \right) - \frac{\omega^{*2} p}{\rho^* c^{*2}} = Q_m. \tag{1}$$

In Eq. (1), $p = p(\mathbf{r}, \omega_r)$ is the acoustic pressure field distribution generally as a function of the position vector $\mathbf{r}$ and real-valued angular frequency ω_r; $\boldsymbol{q}_d = \boldsymbol{q}_d(\mathbf{r}, \omega_r)$, and $Q_m = Q_m(\mathbf{r}, \omega_r)$ represents the dipole and monopole domain sources, respectively; $\rho^* = \rho^*(\mathbf{r}, \omega_r)$, $c^* = c^*(\mathbf{r}, \omega_r)$, and ω^* refer to the density, speed of sound, and angular frequency, respectively, where the superscript "*" means that they can be complex-valued. Those two material parameters are position- and frequency-dependent as well, allowing the consideration of not only spatial variation and frequency dispersion but also potential dissipative loss (e.g., thermal and viscous losses) and/or amplifying gain (e.g., electro-thermo-acoustic coupling) effects. They can even be anisotropic if necessary (*viz.*, rewritten into tensor forms). The frequency, $\omega^* = \omega_r + i\omega_i$, is also set as complex-valued to cope with the case of complex frequency excitation (CFE) that corresponds to time-domain wave with either temporal exponential decay ($\omega_i > 0$) or growth ($\omega_i < 0$).

By solving Eq. (1) for the physical model under consideration at a specific value of ω^* together with necessary boundary conditions, one can obtain the complex-frequency response of the entire computational domain. The complex frequency plane analysis of a scattering system has usually been done by firstly deriving the explicit theoretical model and then performing calculation throughout the complex frequency plane [9,33]. But this becomes unfeasible any more for models without analytical solution, as most finite element method and boundary element method solvers, albeit capable of dealing with complicated systems, do not support complex frequency calculation. Similar issues were encountered for the study of virtual gain and/or loss, in which the practical implementation of CFE in both simulation and experiment relies on truncated yet quasi-steady-state time-domain signal to mimic the complex frequency signal with original form $e^{i\omega^* t} = e^{-\omega_i t} e^{i\omega_r t}$ that is infinitely extended and divergent in time [14,15,23]. Alternatively, the Fourier series expansion

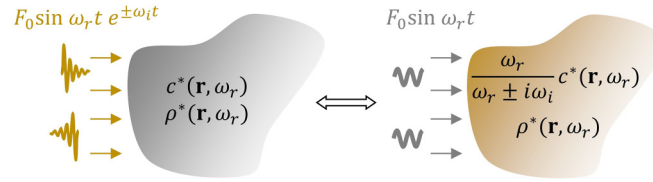

FIG. 1. Schematic illustration of the proposed method for complex frequency calculation. The required complex frequency excitation can be equivalently implemented under real frequency excitation by converting the imaginary frequency component into material parameters.

of the truncated signal at a large number of immediate real frequencies can be combined to synthesize the complex-frequency signal in the frequency domain [15,16]. While those numerical methods are directly related to their experimental realizations, they are often time-consuming and inefficient for early-stage analysis and mechanism exploration. The information loss brought by transient signal truncation and Fourier spectrum discretization could also reduce the performance of CFE [15].

Here we address the aforementioned issues in complex frequency calculation by applying a simple mathematical "trick" to Eq. (1), that is, by converting the imaginary part of frequency, ω_i, representing the exponential decay or growth, into the material parameters in an equivalent manner [34], as illustrated in Fig. 1. Specifically, let $c^* = \frac{\omega^*}{\omega_r} c^*_{\mathrm{eq}}$, and substituting it into Eq. (1) yields

$$\nabla \cdot \left(-\frac{1}{-\rho^*} (\nabla p - \boldsymbol{q}_d) \right) - \frac{{\omega_r}^2 p}{\rho^* {c^*_{\mathrm{eq}}}^2} = Q_m, \tag{2}$$

in which c^*_{eq} denotes the equivalent speed of sound that takes the form

$$c^*_{\mathrm{eq}} = \frac{\omega_r}{\omega^*} c^*. \tag{3}$$

Note that Eq. (2) now only contains harmonic excitation at a purely real frequency. Equations (1) and (2) are fully equivalent and therefore share the same solution. Such treatment transforms a system under CFE into an equivalent system under real-frequency excitation, which can be readily solved by any real-frequency numerical solvers. It is worth mentioning that here we take the Helmholtz equation governing acoustic waves as a specific example, and similar treatments may also be applied to other wave systems or equations such as Maxwell's and Navier-Stokes equations.

Below, the effectiveness of the proposed method is validated by two classes of problems involving complex-frequency calculation, including the complex frequency plane analysis of a one-port resonant scattering system and the complex frequency wave propagation in a lossy holey-structured metamaterial lens. The calculations throughout this manuscript are performed with the frequency domain solver built in COMSOL Multiphysics (v6.2), during which the real frequency, ω_r, and equivalent speed of sound, c^*_{eq}, are utilized to achieve the required CFE.

Complex frequency plane analysis of a scattering system. The eigenvalue poles and zeros of a system's scattering

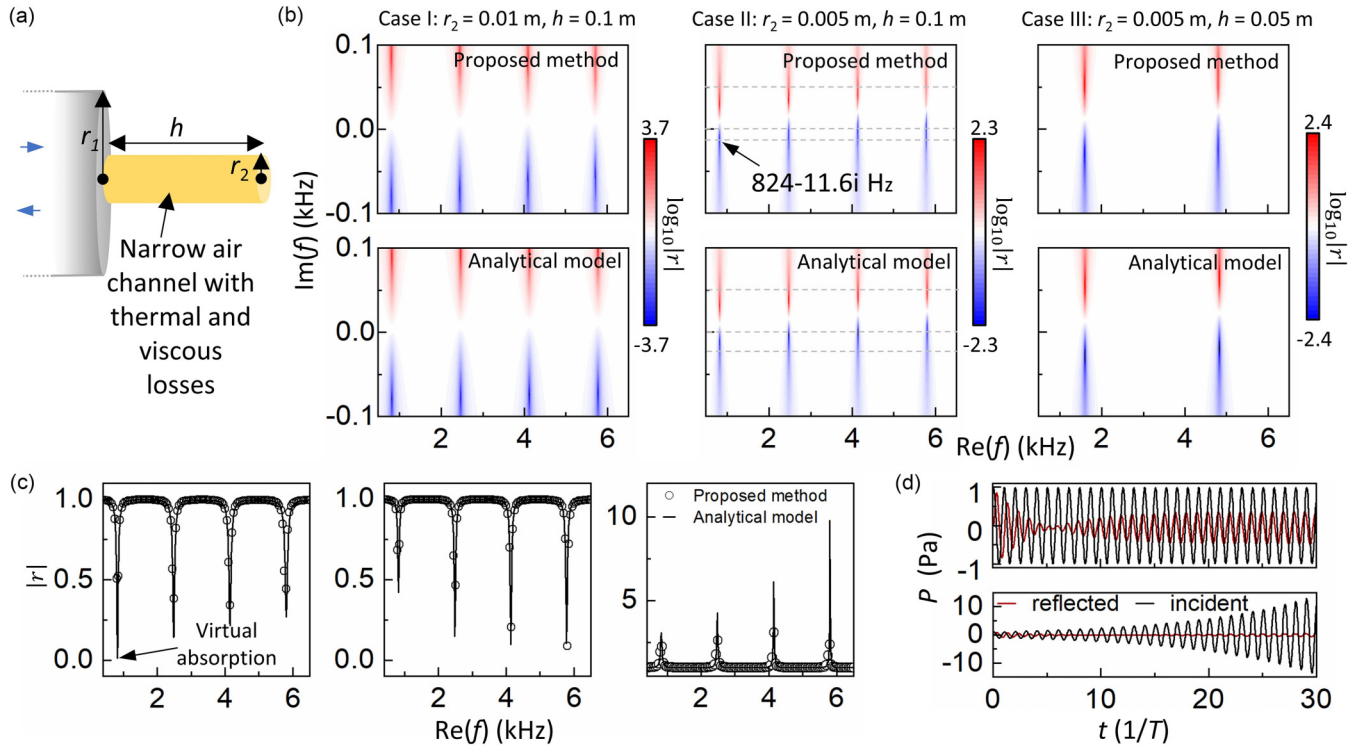

FIG. 2. Complex frequency plane analysis for a one-port acoustic scattering system with thermal and viscous losses. (a) Schematic of the one-port scattering system consisting of a quarter-wavelength resonant cavity (yellow region) connected to a wide circular tube (gray region). (b) Reflection coefficients of three cases in the complex frequency plane in logarithmic scales. The results on top panels are obtained from the proposed method, while the bottoms are from the analytical model. (c) Three selected spectra in case II (marked by the gray dashed lines) for three different imaginary frequencies. (d) Time-domain simulation of virtual perfect absorption. The location of the complex zero excited in the simulation is marked by the black arrows in (b) and (c).

matrix fully reflect its scattering properties [1]. Their locations within the complex frequency plane are usually determined by performing a frequency sweeping along both its real and imaginary axes. We consider the one-port acoustic scattering problem of a lossy quarter-wavelength resonant cavity [Fig. 2(a)], a typical resonant component widely used in sound-absorbing structures [35], and perform complex frequency plane analyses using both our proposed method and the available analytical model [13]. For such one-port systems, the eigenvalue of the scattering matrix is its reflection coefficient, and the zeros of scattering matrix coincide with the scattering zeros suggesting perfect absorption.

The one-port acoustic system consists of a wide circular tube (cross-sectional radius $r_1 = 0.025$ m) connected with a resonant cavity (cross-sectional radius $r_2 < r_1$ and length h) [Fig. 2(a)]. The wide tube is lossless and only supports plane-wave mode in the frequency range of interest. The inherent dissipative loss induced by the viscous and thermal acoustic boundary layer effect inside the cavity is described by the low reduced frequency (LRF) model [36], in which the frequency-dependent dissipation effect is included in the effective speed of sound and density of air. Plane-wave radiation condition is applied at the left end to generate a right-going incident plane wave and to eliminate unwanted reflection from the boundary of the computational domain, consistent with the analytical model for reflection coefficient calculation.

Three cases with different structural parameters are considered to evaluate the validity of our proposed method [Figs. 2(b) and 2(c)]. In all three cases, evidently the results obtained from our proposed method agree perfectly with those from the analytical model (see detailed formula in Ref. [37]), no matter in terms of the positions of zeros and poles [Fig. 2(b)] or the overall refection spectra [Fig. 2(c)]. For longer cavity length $h = 0.1$ m (Cases I and II), four pairs of zeros and poles exist within the interested frequency range, whose real frequencies correspond to the odd integers of quarter wavelength. As expected, the intrinsic dissipative loss indeed breaks the time-reversal symmetry and leads to the asymmetric distribution of poles and zeros about the real axis [1] (conjugate poles and zeros in the lossless case). This asymmetry grows with increased dissipative loss owing to stronger acoustic boundary layer effect in narrower air channels (comparison between Cases I and II). For shorter cavity length $h = 0.05$ m (Case III), less pairs of zeros and poles can be found in the same range due to increased quarter-wavelength resonance frequencies.

Moreover, a time-domain simulation is performed using the thermoviscous acoustic module based on a full linearized Navier-Stokes model to further verify the above frequency-domain results [Fig. 2(d)]. We take the virtual excitation of the

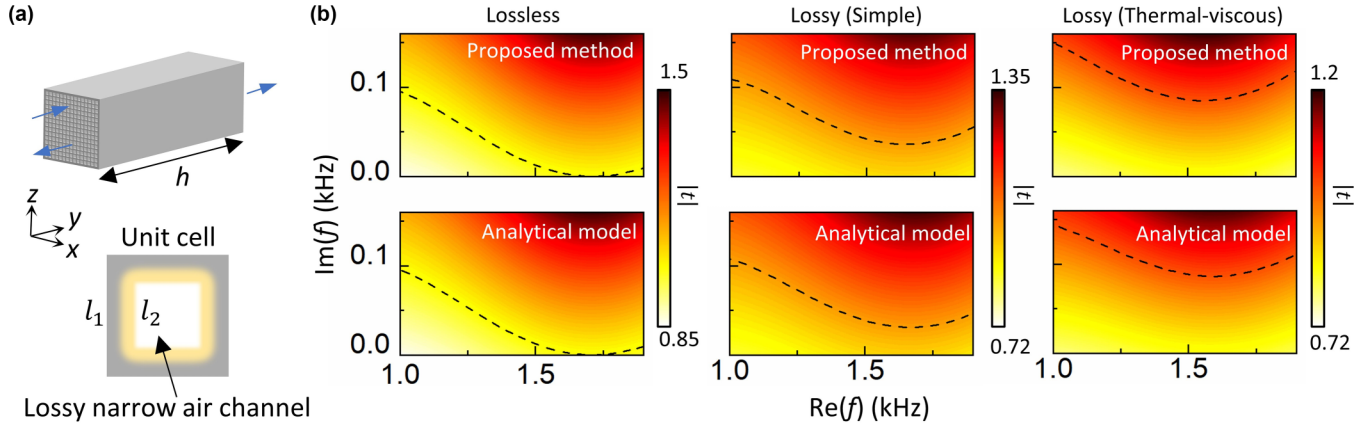

FIG. 3. Transmission characteristics of the holey-structured metamaterial. (a) Schematic of the holey-structured metamaterial working as an acoustic superlens. The lower panel indicates the inherent losses induced by the thermal-viscous boundary layer effect inside the air channel. (b) Transmission coefficients of the lossless (left column) and lossy (middle and right columns) cases within the complex frequency plane. The inherent losses are considered in both a simple way (general dissipation model, middle column) or a more realistic way (the low reduced frequency model of thermal-viscous boundary layer effect [36], right column). The top panels are results obtained from our proposed method, while the bottom ones are from the analytical model. The contour lines of the unitary transmission are marked by the black dashed lines.

first zero located at $824-11.6i$ Hz [black arrows in Figs. 2(b) and 2(c)] in Case II as an example and examine the perfect absorption behavior ($|r| = 1$). By injecting a temporal signal at this complex frequency, $p(t) = \cos(\omega_r t)e^{\omega_i t}$, the incident wave to the cavity is almost totally absorbed as evidenced by the vanishing reflected signal [bottom panel of Fig. 2(d)]. In contrast, considerable wave reflects back under harmonic excitation at the real frequency with incident signal $p(t) = \cos(\omega_r t)$ [upper panel of Fig. 2(d)].

Complex frequency wave propagation in a lossy acoustic metamaterial lens. Recent studies have shown that CFE with temporal exponential decay can supply virtual gain for superlensing systems to overcome their intrinsic dissipative losses that fundamentally limit the super-resolution effect [14,15]. Here we adopt the holey-structured acoustic metamaterial in Refs. [14] and [38] to test the effectiveness of our proposed method in evaluating the response of the acoustic superlens under CFE.

The acoustic superlens, a holey-structured metamaterial, consists of 15 × 15 square through holes arranged periodically within the transverse plane, in which the periodicity, side length, and width are denoted by l_1, l_2, and h, respectively [Fig. 3(a)]. We set $l_1 = 0.02$ m, $l_2 = 0.015$ m, and $h = 0.1$ m, in consistent with Ref. [14]. An analytical model has been derived to evaluate the transmission coefficient of the holey-structured metamaterial [37]. Meanwhile, for direct comparison, we consider the general dissipation model (named "simple lossy") adopted by Ref. [14] to describe the inherent dissipative loss, that is, by utilizing a complex speed of sound $c_c = c\sqrt{1 + i\omega\delta/c^2}$ and a complex density $\rho_c = \rho c^2/c_c^2$, where δ denotes the sound diffusivity and is set as 0.4 m^2/s in the simulation. To demonstrate the versatility of our proposed method, we also provide the results for the LRF model [36] (named "thermal-viscous") that characterizes the dispersion and dissipation of thermal-viscous effect more realistically.

The calculated transmission coefficients of the metamaterial within the complex frequency plane for normal incidence are given in Fig. 3(b). Again, we compare the results obtained from our proposed method [top panels in Fig. 3(b)] with those from the analytical model [lower panels in Fig. 3(b)], which shows excellent agreement for all lossless and lossy cases. As discussed in previous works [14,38], the contour line (black dashed line) of unitary transmission ($|t| = 1$) can touch the real axis around the Fabry-Perot (FP) resonance in the lossless case [leftmost panels of Fig. 3(b)], while it cannot in the lossy case [right two columns of panels of Fig. 3(b)], which suggests attenuated evanescent waves and weakened subwavelength imaging effect due to dissipative loss under real frequency excitation (RFE). This fundamental limit can be overcome by employing CFE to compensate the loss and recover the super resolution.

We further examine the recovered resolution of the superlens under CFE by considering an object to be imaged similar to that in Ref. [14] [upper panel of Fig. 4(a)]. The object (image) plane is 0.5 mm away from the input (output) surfaces of the superlens, sufficiently close to the metamaterial so that the near-field evanescent waves can be tunneled (collected). In the lossless case, a nearly perfect image with deep subwavelength resolution can be obtained at the FP resonance [38] [bottom panel of Fig. 4(a)]. But with the dissipative losses coming into play, the image is blurred for RFE as a result of the attenuation of evanescent wave carrying rich high spatial frequency information [leftmost panels of Fig. 4(b) and 4(c)]. Under CFE, the image quality gradually approaches that of the ideal lossless case as the imaginary part of the excitation frequency increases until the intrinsic losses are exactly compensated at $1705 + 30i$ Hz for the simple lossy model [Fig. 4(b)] and at $1614 + 83i$ Hz for the thermal-viscous model [Figs. 4(c) and 4(d)]. The latter has been regarded as a more realistic description of the inherent thermal-viscous losses, in which a red shift of FP resonance appears due to the reduced effective speed of sound from dispersion [36,39,40].

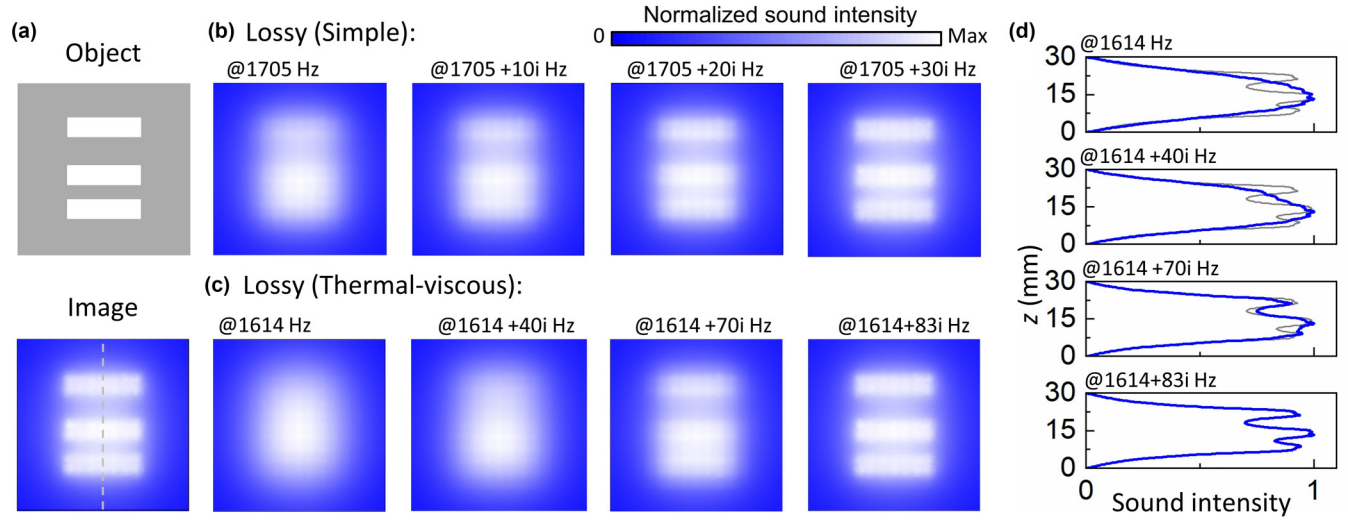

FIG. 4. Imaging of a lossy acoustic superlens under complex frequency excitation. (a) The object to be imaged (top) and the image of the lossless case under real frequency excitation (bottom). [(b),(c)] The images obtained through the proposed method at different complex frequencies. Two lossy models, the simple lossy model (b) and thermal-viscous model (c), are considered. (d) Image cut of normalized sound intensity at the gray dashed line marked in (a) for the thermal-viscous model, in which the gray (blue) solid line is for the ideal lossless (lossy) case.

As compared to the time-domain method adopted in Refs. [14,23] and the multifrequency synthetization method adopted in Refs. [15,16] for complex frequency calculation (though they are important experimental methods), our proposed method shows advantages in computational efficiency, capability of dealing with complex dispersion and loss, and conciseness of post data processing (see detailed comparison and discussions in [37]). Most importantly, since our proposed method is basically free of the information loss during transient signal truncation, establishment of quasisteady state, or discretization of Fourier spectrum (at least one of which is necessary for the other two methods), it actually represents the most accurate complex frequency response of the system that the other two methods can only approach but never exceed.

Discussion and conclusion. To conclude, we have proposed a numerical method to conduct complex-frequency calculation for acoustic systems, in which the required complex frequency is equivalently transformed into complex material parameters so that the calculation can be performed by real-frequency solvers. Two typical classes of problems, including the complex frequency plane analysis of a one-port scattering system and the complex frequency wave propagation in a lossy acoustic metamaterial lens, have been considered with a detailed comparison with the results from the analytical models. The results well confirm the effectiveness and flexibility of our proposed method. In light of the fact that our proposed method in essence converts the imaginary frequency component into an additional variation in material parameters, it is in principle applicable to any linear, time-invariant acoustic systems provided that the associated computation for the complex material parameters is allowed in the numerical solver that we adopt, even in some extreme situations (e.g., irregular cavities and invisible poles [41]), as discussed in the Supplemental Material [37] (see also Refs. [42–46] therein). Our work therefore provides an elegant solution to the characterization and evaluation of open scattering and, in general, non-Hermitian systems involving complex frequency calculation, which can also be further extended to other wave systems or other forms of equations like Maxwell's equation and Navier-Stokes equation.

Acknowledgments. We thank Professor Y. Peng from Huazhong University of Science and Technology for the discussions on acoustic superlens. T.L. acknowledges support from the National Natural Science Foundation of China (Grant No. 12104383) and the Basic and Frontier Exploration Project Independently Deployed by Institute of Acoustics, Chinese Academy of Sciences (Grant No. JCQY202403). J.Z. acknowledges support from the Research Grants Council of Hong Kong SAR (Grant No. AoE/P-502/20), the Fundamental Research Funds for the Central Universities and the National Natural Science Foundation of China (Grant No. 92263208).

Data availability. The data that support the findings of this article are not publicly available upon publication because it is not technically feasible and/or the cost of preparing, depositing, and hosting the data would be prohibitive within the terms of this research project. The data are available from the authors upon reasonable request.

[1] A. Krasnok, D. Baranov, H. Li, M.-A. Miri, F. Monticone, and A. Alú, Anomalies in light scattering, Adv. Opt. Photonics **11**, 892 (2019).

[2] Z. Gu, H. Gao, P.-C. Cao, T. Liu, X.-F. Zhu, and J. Zhu, Controlling sound in non-Hermitian acoustic systems, Phys. Rev. Appl. **16**, 057001 (2021).

[3] C. W. Hsu, B. Zhen, A. D. Stone, J. D. Joannopoulos, and M. Soljačić, Bound states in the continuum, Nat. Rev. Mater. **1**, 16048 (2016).

[4] S. Qu and P. Sheng, Microwave and acoustic absorption metamaterials, Phys. Rev. Appl. **17**, 047001 (2022).

[5] L. Huang, S. Huang, C. Shen, S. Yves, A. S. Pilipchuk, X. Ni, S. Kim, Y. K. Chiang, D. A. Powell, J. Zhu, Y. Cheng, Y. Li, A. F. Sadreev, A. Alù, and A. E. Miroshnichenko, Acoustic resonances in non-Hermitian open systems, Nat. Rev. Phys. **6**, 11 (2024).

[6] S. Huang, Y. Li, J. Zhu, and D. P. Tsai, Sound-absorbing materials, Phys. Rev. Appl. **20**, 010501 (2023).

[7] A. Canós Valero, H. K. Shamkhi, A. S. Kupriianov, T. Weiss, A. A. Pavlov, D. Redka, V. Bobrovs, Y. Kivshar, and A. S. Shalin, Superscattering emerging from the physics of bound states in the continuum, Nat. Commun. **14**, 4689 (2023).

[8] S. Kim, S. Lepeshov, A. Krasnok, and A. Alù, Beyond bounds on light scattering with complex frequency excitations, Phys. Rev. Lett. **129**, 203601 (2022).

[9] C. Wang, W. R. Sweeney, A. D. Stone, and L. Yang, Coherent perfect absorption at an exceptional point, Science **373**, 1261 (2021).

[10] L. Ge, Y. D. Chong, and A. D. Stone, Conservation relations and anisotropic transmission resonances in one-dimensional PT-symmetric photonic heterostructures, Phys. Rev. A **85**, 023802 (2012).

[11] W. R. Sweeney, C. W. Hsu, S. Rotter, and A. D. Stone, Perfectly absorbing exceptional points and chiral absorbers, Phys. Rev. Lett. **122**, 093901 (2019).

[12] V. Romero-García, N. Jimenez, G. Theocharis, V. Achilleos, A. Merkel, O. Richoux, V. Tournat, J.-P. Groby, and V. Pagneux, Design of acoustic metamaterials made of Helmholtz resonators for perfect absorption by using the complex frequency plane, C. R. Phys. **21**, 713 (2020).

[13] V. Romero-García, G. Theocharis, O. Richoux, and V. Pagneux, Use of complex frequency plane to design broadband and sub-wavelength absorbers, J. Acoust. Soc. Am. **139**, 3395 (2016).

[14] S. Kim, Y.-G. Peng, S. Yves, and A. Alù, Loss compensation and superresolution in metamaterials with excitations at complex frequencies, Phys. Rev. X **13**, 041024 (2023).

[15] F. Guan, X. Guo, K. Zeng, S. Zhang, Z. Nie, S. Ma, Q. Dai, J. Pendry, X. Zhang, and S. Zhang, Overcoming losses in superlenses with synthetic waves of complex frequency, Science **381**, 766 (2023).

[16] F. Guan, X. Guo, S. Zhang, K. Zeng, Y. Hu, C. Wu, S. Zhou, Y. Xiang, X. Yang, Q. Dai, and S. Zhang, Compensating losses in polariton propagation with synthesized complex frequency excitation, Nat. Mater. **23**, 506 (2024).

[17] Z. Gu, H. Gao, H. Xue, J. Li, Z. Su, and J. Zhu, Transient non-Hermitian skin effect, Nat. Commun. **13**, 7668 (2022).

[18] K. Zeng, C. Wu, X. Guo, F. Guan, Y. Duan, L. L. Zhang, X. Yang, N. Liu, Q. Dai, and S. Zhang, Synthesized complex-frequency excitation for ultrasensitive molecular sensing, eLIGHT **4**, 1 (2024).

[19] H. Li, A. Mekawy, A. Krasnok, and A. Alù, Virtual parity-time symmetry, Phys. Rev. Lett. **124**, 193901 (2020).

[20] D. G. Baranov, A. Krasnok, and A. Alù, Coherent virtual absorption based on complex zero excitation for ideal light capturing, Optica **4**, 1457 (2017).

[21] C. Rasmussen, M. I. N. Rosa, J. Lewton, and M. Ruzzene, A lossless sink based on complex frequency excitations, Adv Sci. **10**, 2301811 (2023).

[22] Y. Ra'di, A. Krasnok, and A. Alù, Virtual critical coupling, ACS Photonics **7**, 1468 (2020).

[23] G. Trainiti, Y. Ra'di, M. Ruzzene, and A. Alù, Coherent virtual absorption of elastodynamic waves, Sci. Adv. **5**, eaaw3255 (2019).

[24] A. Farhi, A. Mekawy, A. Alù, and D. Stone, Excitation of absorbing exceptional points in the time domain, Phys. Rev. A **106**, L031503 (2022).

[25] A. Archambault, M. Besbes, and J.-J. Greffet, Superlens in the time domain, Phys. Rev. Lett. **109**, 097405 (2012).

[26] M.-A. Miri and A. Alù, Exceptional points in optics and photonics, Science **363**, 42 (2019).

[27] S. K. Ozdemir, S. Rotter, F. Nori, and L. Yang, Parity-time symmetry and exceptional points in photonics, Nat. Mater. **18**, 783 (2019).

[28] R. El-Ganainy, K. G. Makris, M. Khajavikhan, Z. H. Musslimani, S. Rotter, and D. N. Christodoulides, Non-Hermitian physics and PT symmetry, Nat. Phys. **14**, 11 (2018).

[29] K. Ding, C. Fang, and G. Ma, Non-Hermitian topology and exceptional-point geometries, Nat. Rev. Phys. **4**, 745 (2022).

[30] E. J. Bergholtz, J. C. Budich, and F. K. Kunst, Exceptional topology of non-Hermitian systems, Rev. Mod. Phys. **93**, 015005 (2021).

[31] X. Zhang, F. Zangeneh-Nejad, Z.-G. Chen, M.-H. Lu, and J. Christensen, A second wave of topological phenomena in photonics and acoustics, Nature (London) **618**, 687 (2023).

[32] D. T. Blackstock, *Fundamentals of Physical Acoustics* (Wiley, New York, 2000).

[33] Z. Zhou, S. Huang, D. Li, J. Zhu, and Y. Li, Broadband impedance modulation via non-local acoustic metamaterials, Natl. Sci. Rev. **9**, nwab171 (2021).

[34] Q. Bai, M. Perrin, C. Sauvan, J. P. Hugonin, and P. Lalanne, Efficient and intuitive method for the analysis of light scattering by a resonant nanostructure, Opt. Express **21**, 27371 (2013).

[35] M. Yang, S. Chen, C. Fu, and P. Sheng, Optimal sound-absorbing structures, Mater. Horiz. **4**, 673 (2017).

[36] W. R. Kampinga, Viscothermal Acoustics Using Finite Elements-Analysis Tools for Engineers, Ph.D. thesis, University of Twente, 2010.

[37] See Supplemental Material at http://link.aps.org/supplemental/10.1103/PhysRevB.111.L020301 for the complex frequency analyses in two extreme situations, comparison of the proposed method with the time-domain and multifrequency synthesization methods, involved analytical derivations, and simulation details.

[38] J. Zhu, J. Christensen, J. Jung, L. Martin-Moreno, X. Yin, L. Fok, X. Zhang, and F. J. Garcia-Vidal, A holey-structured metamaterial for acoustic deep-subwavelength imaging, Nat. Phys. **7**, 52 (2011).

[39] F. Mbailassem, E. Gourdon, Q. Leclère, E. Redon, and T. Cambonie, Sound absorption prediction of linear damped acoustic resonators using a lightweight hybrid model, Appl. Acoust. **150**, 14 (2019).

[40] M. R. Stinson, The propagation of plane sound waves in narrow and wide circular tubes, and generalization to uniform tubes

of arbitrary cross-sectional shape, J. Acoust. Soc. Am. **89**, 550 (1991).

[41] D. Trivedi, A. Madanayake, and A. Krasnok, Revealing invisible scattering poles via complex frequency excitations, arXiv:2408.09617.

[42] D.-Y. Maa, Potential of microperforated panel absorber, J. Acoust. Soc. Am. **104**, 2861 (1998).

[43] M. R. Stinson and E. A. G. Shaw, Acoustic impedance of small, circular orifices in thin plates, J. Acoust. Soc. Am. **77**, 2039 (1985).

[44] Y. Li and B. M. Assouar, Acoustic metasurface-based perfect absorber with deep subwavelength thickness, Appl. Phys. Lett. **108**, 063502 (2016).

[45] S. An, T. Liu, L. Cao, Z. Gu, H. Fan, Y. Zeng, L. Cheng, J. Zhu, and B. Assouar, Multibranch elastic bound states in the continuum, Phys. Rev. Lett. **132**, 187202 (2024).

[46] S. Huang, T. Liu, Z. Zhou, X. Wang, J. Zhu, and Y. Li, Extreme sound confinement from quasibound states in the continuum, Phys. Rev. Appl. **14**, 021001(R) (2020).